Manipulation of superconductivity in van der Waals materials and thin films

Chen, X.

7

TOWARDS ARTIFICIAL FOLDING OF THE ELECTRONIC BANDS IN MgB_2

We explore the possibility of measuring the effect of electronic band folding in MgB_2 with a charge transport study. We successfully fabricate superconducting current constrictions with widths below 1 μm using a Gallium focused ion beam. A periodic pattern with a periodicity of about 100 nm is then imprinted on the device surface to induce electronic band folding. According to theoretical predictions, this will increase the phase space for electron phonon coupling, which results in an increase in critical temperature. This was, however, not observed in our experiments. Upon quantitatively analysing our data, we do find that the periodic pattern could potentially bring benefits that makes the device more resilient against damage by the focused ion beam. We give a detailed prospect for possible future projects regarding the topic.

7.1. INTRODUCTION

In solid-state physics, the electronic band structure is a key factor for materials' properties. Making artificial materials with novel quantum properties by altering and reshaping a pristine material's electronic band has been a popular topic in modern condensed matter physics [160] [161] [162] as well as nanotechnology [96] and chemistry [163] [164].

Reshaping the electronic band can be done in different ways. A recent example is the twist-and-stack van der Waals heterostructures. For example, by hybridising two individual electronic bands from two separate monolayer graphene at a given twist angle, the so-called magic angle, it is possible to create an ultra-flat electronic band leading to strongly correlated electron behaviour [165]. The system can then be tuned into the superconducting regime either by applying an electric gate voltage or a magnetic field [15].

Equivalently, these results can be interpreted by moiré physics, through the effect of band folding due to a larger periodic potential with a periodicity that is several times the original lattice constant [166]. Band folding refers to how the electronic band structure reacts to a supercell potential. As the periodicity of the electron potential in real space increases, the first Brillouin zone in reciprocal space decreases in size, causing the original band that crosses the new Brillouin zone boundary to fold back and further populate the zone. At the edge of the newly defined, smaller Brillouin zone, band gaps are expected

to open up due to Bragg scattering, giving opportunities for the formation of flat bands where electrons have low kinetic energy. For van der Waals materials, the twist-and-stack method can create a moiré periodicity that is much larger than the original primitive cell. For instance, twisted bi-layer graphene at the first magic angle of 1.1° has a moiré periodicity of 23.8 nm, around fifty times larger than its primitive lattice constant. The moiré periodicity acts as the supercell potential, folding back the original electronic bands, and creating ultra flat bands in magic-angle twisted bilayer graphene.

For a material that already exhibits superconductivity, imposing a superperiodicity on top of its original lattice constant has the potential to enhance the superconducting phase parameters by strengthening phonon-electron coupling near the Fermi level in conventional, phonon-mediated superconductors [167] [168] [169] [170]. This is a direct consequence of the enlargement in the phase space for electron-phonon interaction [167]. Experimentally the superconducting critical temperature is expected to rise by an observable amount. An "improved" superconductor with a higher critical temperature can therefore be realised.

As previously mentioned, the creation of flat bands has been observed in van der Waals materials where the superperiodicity is created by moiré patterns generated by either a layer with a different orientation [37] or a layer of a different type [171] [172]. A metamaterial superconductor was also reported where a higher critical temperature can be created by layering the superconductor with an insulator [169] [170].

Here, we explore the possibility of creating supercells with an alternative method. To this end, we perform direct periodic patterning on MgB_2 with Focused Ion Beam milling (FIB) and investigate how the patterns influence the transport properties of the devices.

Parameter	Experimental Values	Theoretical Values
Coherence length ξ (0)	3.7 – 12 nm (ab) / 1.6 – 3.6 nm (c)*	
Penetration depths λ (0)	85 - 180 nm*	39.2 nm (clean) / 105.7 nm (dirty)**
Energy gaps Δ (0)	5.5 – 8.2 meV (σ) / 1.5 – 3.5 meV (π)***	7.09 meV (σ) / 2.70 meV (π) ***
Upper critical field H_{c2} (0)	14 – 39 T (ab) / 2 – 24 T (c)*	
Critical temperature	39 - 40 K****	

Table 7.1: (a) List of superconducting parameters of MgB2 *[173]; **[174]; ***[151] [175] [176] [177] [96] [178]; ****[179].

MgB_2 is well-known as a material that has the highest critical temperature in phonon-mediated superconductors [179]. The values of some relevant superconducting parameters are listed in Table 7.1. MgB_2 is a multi-gap superconductor with a high cooper pair density [180]. It was understood only a very small percentage of the phonons in the system contributes to the pairing of electrons in this superconductor [181]. This makes it a suitable candidate for investigating the possible rise of the of the critical temperature caused by the increase in phase space for electron-phonon coupling induced by band folding. As MgB_2 is commonly epitaxially grown as a crystalline film superconductor, the periodic potential may not be realised by another layer of MgB_2 or molecules. Instead, it is more logical to create a periodic pattern in the thin film itself, reminescent of the concept to create and tune photonic bands in optical materials with a periodic structure

[182].

The periodicity of the artificial lattice structure needs to be within a range that is achievable by the modern state-of-the-art nano-fabrication process while being meaningful for the band folding picture. Theoretically, the imposed periodicity should be at least several times larger than the size of the pristine unit cell. Nevertheless, if the supercell is too large, the new Brillouin zone becomes very small, forcing all electronic bands to be closer and closer together. This will encourage unwanted umklapp scattering, which destroys superconductivity [167]. The limitation mainly comes from nano-fabrication methods. That puts the estimated patterning resolution to be around 50-80 nm. FIB presents a promising solution for high-resolution patterning devices. Still unfortunately, it has been reported that FIB structuring damages the sample, and therefore could decrease the critical temperature and critical current of the devices [129] [183]. Hence, it is important to investigate the sample quality at each step in the fabrication process.

In this chapter, we present the properties of superconducting MgB_2 nano-bridge devices patterned with FIB. With Pt as the protective layer, we managed to fabricate superconducting nano-bridges down to 600 nm in width. We then patterned periodic structures on the nano-bridge and studied how this influence the transport properties of the devices. We did not observe an increase in critical temperature after a periodic pattern was imposed on the device. However, through the comparison of the quantitative analysis between two separate devices, it was realised that the periodic pattern could potentially be more resilient to the damage of FIB. With this in mind, we present an outlook on the possible future directions of manually folding band structures in superconductors hoping to inspire more studies in this field.

7.2. FABRICATION METHOD

The 50 nm thick MgB_2 epitaxial films were grown on 6H-SiC(0001) substrates (Temple University, USA). The films were then transferred to an electron beam evaporator, and 50 nm of platinum was deposited on top as a protective layer for further fabrication process. A standard electron beam lithography method with AR-P 6200 (CSAR 62) as the positive resist was used to define a microstrip pattern (width $\approx$ 10 μm) with a 4 terminal contacts arrangement. The pattern was transferred to the thin film using argon etching in a K-cell etcher (P_{Ar} = 4 E -4 mbar, Etching time = 9 min). Electrical measurements (resistance, I-V curves) were performed on this microstrip for temperatures down to 36 K, well below the critical temperature of the MgB_2 film.

After initial characterisation, constrictions for the current with widths in the order of 1 μm were milled through with a Gallium FIB (30 keV). The optical microscope image of a typical microstrip is shown in Figure 7.1 (a) inset, and the scanning electron microscope (SEM) image of a typical nano-constriction of the current is shown in Figure 7.1 (a). In this particular device, the current constriction has a width of 0.60 μm $\pm$ 0.05 μm. After the current constriction had been structured, another round of transport measurements was performed to document the changes in the device's electronic properties.

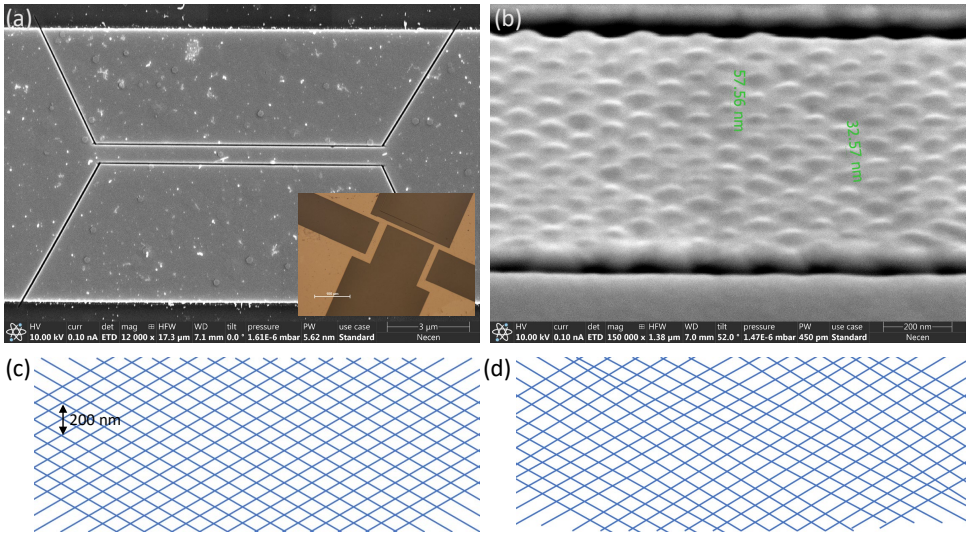

Figure 7.1: (a) Scanning Electron microscope image of the current constriction made with FIB. The width for this particular device is 0.60 μm ± 0.05 μm, inset shows the optical image of the argon etched microbridge (width = 9.7 μm ± 0.1 μm) before the current constriction was milled. (b) Scanning Electron microscope image taken at a 52° tilt of the same current constriction after the pattern. (c) The periodic structure which was milled on one current constriction. The distance between two vertical crossings of the structural lines is 100 nm. (d) The non-periodic structure which was used on a separate current constriction as a control experiment.

It was previously observed that the superconductivity in the device could be very quickly destroyed if the ion beam is in direct contact with the MgB_2 surface [164]. There are also reports where the damage caused by secondary electrons is enough to destroy or largely weaken superconductivity without actual physical removal of the devices [184]. A Monte-carlo simulation (SRIM 2013) of the ion range of 30 keV Ga ions in Pt shows that the Ga ions do not penetrate the 50 nm Pt top cover layer. Upon the process of milling, the protective layer gradually thins down at where the beam has passed, allowing a very small amount of ions to leak into the underlying MgB_2. The results of the SRIM calculation are shown in figure 7.2 for the ion penetration process when the surfaces are protected by Pt of two different thicknesses; 50 nm (a) and 20 nm (b) respectively. The average ion range of 30 keV gallium ion in platinum is around 10 nm. However, there is already a small amount of the ions that penetrate into MgB_2 when the thickness of Pt is 20 nm. Therefore, in order to achieve localised damage in the superconductor without completely destroying the material, a dose test was performed on the device.

The dose test aimed to find the optimal amount of ions injected into the device surface without removing more than 30 nm of the platinum layer. The equivalent dose of FIB is measured in the depth at which a standard Si substrate would be cut into with the same amount of ion. A low beam current of 1.5 pA is used to minimise beam size. Figure 7.2 (b) inset shows an SEM image taken during the dose test. The structured pattern is illustrated as the blue line. At an equivalent dose of 0.05 μm, chunks of platinum are

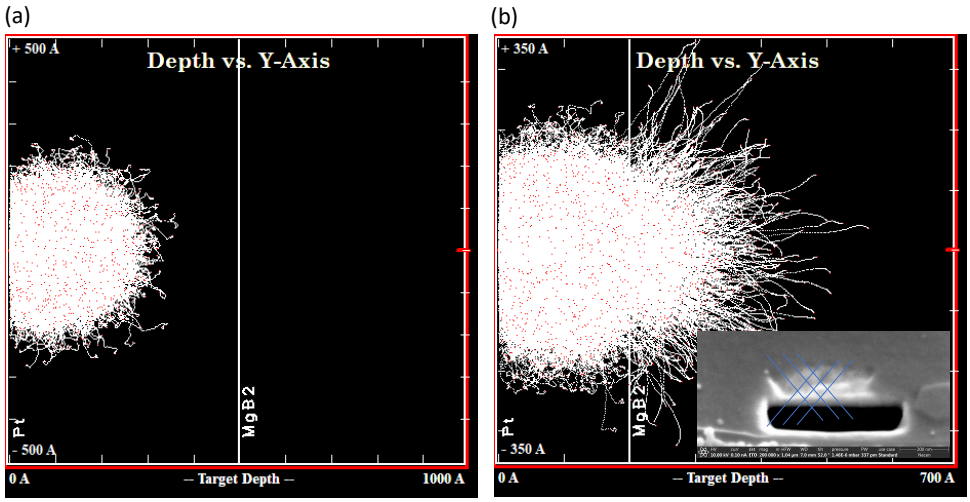

Figure 7.2: (a) Monte Carlo simulation (SRIM2013) ion penetration process after more than 55000 gallium ions for a 50 nm Pt layer on MgB_2. The calculated ion range is 8.3 nm with a struggle (standard deviation) of 5.1 nm. (b) The same calculation for a 20 nm Pt layer on MgB_2. In this case, a small amount of the ion penetrate into the MgB_2 layer. The inset shows an SEM image of the FIB dose test with 0.05 μm FIB dose.

already missing on the surface, leaving behind a rough surface. An equivalent dose of 0.02 μm was chosen eventually for structuring the periodic pattern.

Figure 7.1 (b) shows the SEM image at a 52° tilt of one of the devices with the periodic pattern. The surface in the SEM image is the remaining Pt (~20-30 nm) protective layer. The imprinted periodic pattern is shown in the figure 7.1 (c). Note that the intended periodic structure should consist only of the dots created when the two lines cross, where the damage is the largest to the devices.

If the electron is dominated by the potential well induced by the periodic pattern that is directly structured on top of the current constriction, we expect an increase in the device's critical temperature and critical current. This increase is in competition with the decrease of both values due to the FIB damage to the devices. To differentiate the decrease and the increase due to different causes, we structured two devices exposed during fabrication with exactly the same amount of ion beam periodic pattern and a similar non-periodic pattern that does not have long-range order. In order to include the possible effect of local doping, the area density of the ion beam exposure is kept to be the same for the two devices. The non-periodic pattern is created by rotating the lines in figure 7.1 (c) inset 1° or 2° clockwise or anticlockwise in respect of the original periodic pattern, breaking the local translation symmetry. This non-periodic pattern is shown in the figure 7.1 (d).

We have performed AFM measurements on the sample surface to further study the periodicity (see appendix). However, the results are not conclusive for two reasons. Firstly, the surfaces are still covered with the protective Pt layer. The measured surface topog-

raphy in the AFM does not constitute a measurement of the influence of the FIB on the underlying MgB_2. It can, nevertheless, give a rough map of where the ion beam reaches the furthest. Secondly, the damage of the MgB_2 layer, most likely due to the loss of crystallinity, is not equivalent to the physical removal of Pt on the top. The implication of this is that, the pattern on the surface does not directly reflect the underlying damage done on the MgB_2, which may follow exactly where the beam can reach. For these reasons, the surface measurements from AFM have limited significance in reflecting the condition of the actual devices. We recommend using Transmission Electron Microscopy to further investigate the underlying MgB_2 layer.

7.3. RESULTS AND ANALYSIS

Here, we first show how the initial step of structuring the narrow current constriction with FIB changed the transport properties of the devices. Figure 7.3 (a) shows the temperature

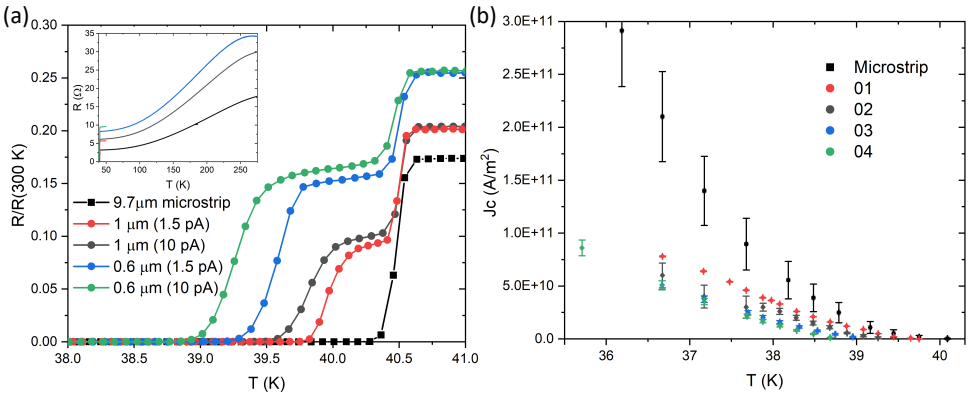

Figure 7.3: (a) Resistance normalised by room temperature resistance as a function of temperature around the transition point for 4 different devices (round symbols) after structured with FIB compared to their original microstrip (square symbols). The label shows the approximate width for each device and at which beam current they had been milled. All devices were milled with the same dose of ion. The inset shows the actual measured resistance-temperature curve. (b) Critical current densities collected at temperatures just below transition temperature for all 4 different devices compared to the microstrip. The same device is represented as the same colour in the two graphs, and we will now refer to them as devices 01-04.

dependence of the residual resistance ratio curves of five different devices of various widths. We compare the 9.7 μm wide wire defined by e-beam lithography and Ar etching with the devices structured by FIB, i.e., 2 wires of 1 μm width and 2 wires of 0.6 μm width using either 1.5 pA or 10 pA ion beam current. Figure 7.3 (b) compares the critical current densities of them with the original microstrip. The data collected from the same devices are represented with the same colour in the two graphs, and in the legend in figure 7.3 (b), where they are further specified as devices 01 to 04, which will be consistently referred as such for the rest of the chapter.

In figure 7.3 (a), we plot the normalised resistance, R(T)/R(300K), in order to compare

the devices directly while the inset shows the actual measured resistance values. We define the critical temperature as the first point in temperature at which the resistance is measured at noise level (about 0.1 mΩ at 10 μA). As can be seen, the critical temperature decreases after the current constrictions are structured. The step-like feature in the resistance transition in the measured resistance as a function of temperature indicates that the FIB damage at the current constriction causes this area to have a lower critical temperature than the rest of the microstrip. As the temperature decreases, the microstrip first becomes superconducting, causing the resistance to drop to the resistance of the current constriction in the normal state. This is also the reason why the observed step in normalised resistance ratio for the devices with thinner widths (devices 03 and 04) have values of about 0.15, whereas for the wider devices, the residual resistance are only about 0.10. As the current constriction itself started to become superconducting, the measured resistance eventually drops down to the noise level, giving the critical temperature for the whole device. From our measurements, it is evident that there is damage that affects device performance for all devices.

When comparing two devices of similar widths, the sample that is structured with higher beam current (10 pA) has a slightly larger measured resistance (the step levels in figure 7.3 (a)) and a lower critical temperature. We attribute this difference to a slightly larger beam size for the 10 pA current, which might lead to more damage to the devices.

The effect of damage is also clearly reflected in the large decrease in critical current density (see figure 7.3 (b)). The details for calculating critical current density are stated in Appendix 7.B. This indicates the supercurrent should flow almost uniformly through the current constriction. Hence, the critical current densities were calculated with the actual cross-sections of the constriction. The decrease in critical current density for the FIB-ed devices is consistent with their drop in critical temperature, signifying there is always damage when the ion beam is used to make the device.

Device 01 is the device structured with the periodic pattern (shown in figure 7.1 (c)). Figure 7.4 shows how the transport properties of this device change after each fabrication process. The schematic of the device geometry is shown in the inset of figure 7.4 (a). From the data we determine the critical temperature to be 0.8 K lower than before any FIB was used on the device after the current constriction has been milled (FIB01). As this part of the device is in series with the rest of the sample (red and black boxes in the inset), the damage is reflected as a step in the resistance temperature curve with a broad transition in temperature. This was discussed before. The critical temperature is further decreased by 0.2 K after the FIB is used again to structure a periodic pattern on top of the current constriction (FIB02). The position of the periodic pattern is indicated by the green box in the inset. The additional FIB milling creates an extra step in the resistance transition, as indicated by the green arrow. The damage here by FIB is more limited, reflected in the relatively small decrease in the critical temperature. As the undamaged part of the microstrip (black box) always transits first, the initial resistive transition starts at the same temperature as the initial microstrip, indicated by the black arrow. The resistance transition also preserves the transition from the current constriction. This is indicated by the red arrow.

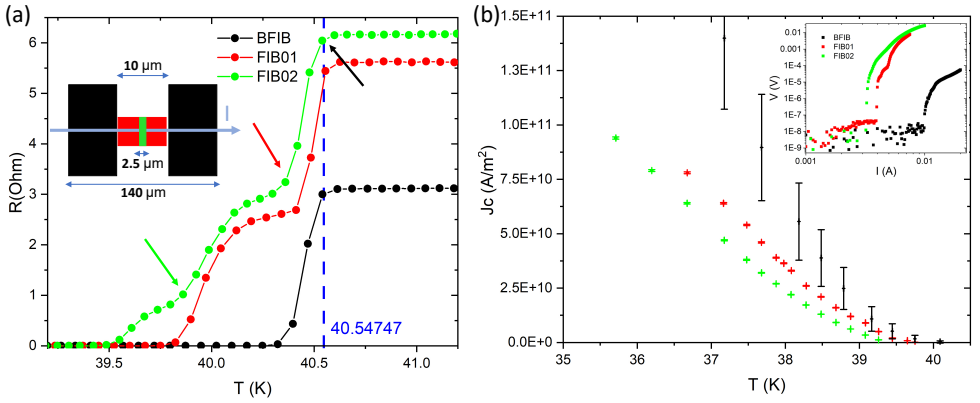

Figure 7.4: (a) Measured resistance as a function of temperature around the transition point for device 01, the inset shows a schematic of the device geometry. (b) Critical current densities collected at temperatures just below transition temperature for device 01 after each fabrication step, the inset shows the I(V) curves collected at 36.7 K of device 1 after each step. The colour scheme corresponds with each other in two graphs. BFIB represents data collected from the microstrip, FIB01 represents after the current constriction was structured, and FIB02 was collected after a periodic pattern is printed on top of the current constriction.

A similar conclusion can be drawn from the critical current measured at different temperatures as plotted in figure 7.4 (b). The inset shows a set of typical I-V curves for device 01 before FIB, after defining the constriction and after creating the periodic pattern; the data here are measured at 36.7 K. The measured critical current only decreased by a small amount after the second round of FIB. This signifies the damage from the second time milling is more limited compared to the first time, in agreement with the resistance transition in temperature. As shown in the data obtained from device 01, the influence of damage dominates the changes in superconducting parameters, the periodic patterning seems to have not improved device performance in any way. To investigate this further, as discussed in the previous section, we next focus on comparing the results obtained from the periodically patterned device with the device that was patterned with the non-periodic structure.

The non-periodic pattern (shown in figure 7.1 (d)) is structured on device 02. To reiterate, the aim here is to differentiate between the effects of damage and the periodic potential. We will also include results obtained from device 03 which has been structured with a smaller periodic pattern (50 nm). It should be noted that SEM images of this device show no obvious periodic pattern which we attribute to drift in the FIB during milling.

Figure 7.5 (a) compares the critical current density as a function of temperature for device 01 (grey), 02 (pink) and 03 (blue) before (FIB01) and after (FIB02) the surfaces were patterned with a nanostructure. The data is then fitted to the Ginzburg-Landau scaling law with a critical exponent α:

$$J_c(T) = J_c(0)\left(1 - \frac{T}{T_c}\right)^{\alpha} \tag{7.1}$$

(a)

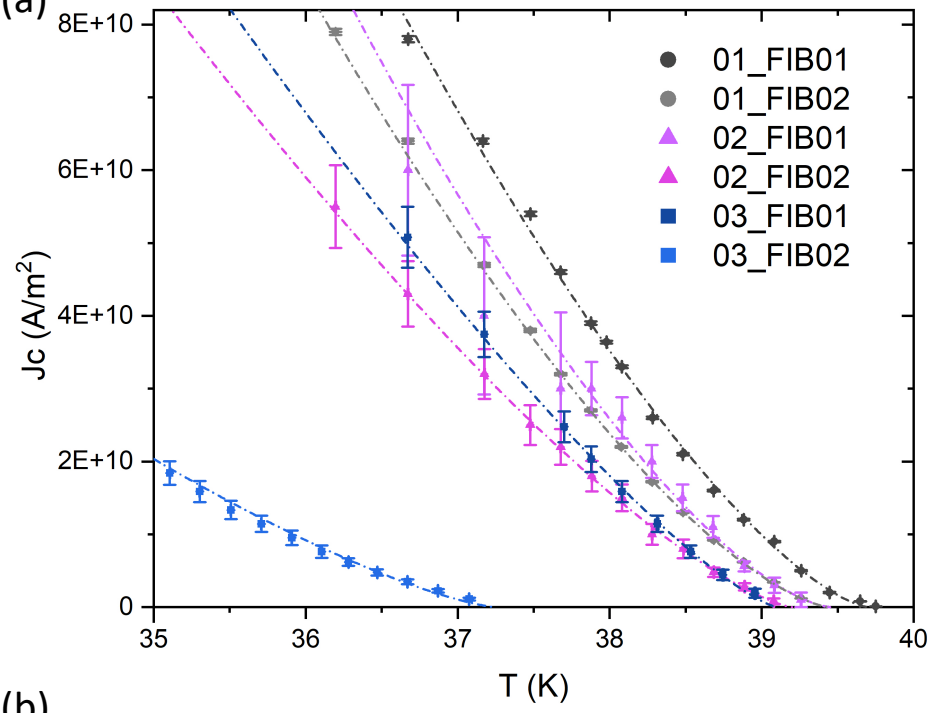

(b)

Device	Width (μm)	Tc (K)	Jc (0) (A/m²)	α
01_FIB01	1.0 ± 0.1	39.7	3.2E12 ± 5E11	1.43 ± 0.05
01_FIB02	1.0 ± 0.1	39.5	3.06E12 ± 8E10	1.47 ± 0.01
02_FIB01	1.0 ± 0.1	39.5	3.6E12 ± 9E11	1.50 ± 0.07
02_FIB02	1.0 ± 0.1	39.3	1.7E12 ± 1E11	1.35 ± 0.02
03_FIB01	0.60 ±0.05	39.1	1.74E12 ± 2E11	1.28 ± 0.03
03_FIB02	0.60 ±0.05	37.2	9.0E11 ± 5E10	1.35 ± 0.02

Figure 7.5: (a) measured critical current density as a function of temperature for Device 01, 02 and 03 before (FIB01) and after (FIB02) a pattern had been structured on the top of the current constriction. The dashed lines are the fitting of the Ginzburg-Landau scaling law to the data points. The fit parameters and critical temperature for each curve are listed in the table in (b).

Where J_c is the critical current density, $J_c(0)$ is the estimated critical current density at zero kelvin, T is the measured temperature and T_c is the critical temperature. The fitting parameters $J_c(0)$ and α for each curve are listed in the table shown in figure 7.5 (b).

We interpret the results as follows. For the superconductor following a perfect second order transition, the critical exponent α is expected to be exactly $3/2$ (standard Ginzburg-Landau model). However, in inhomogeneous superconductors with different characteristic lengths, the transition diverges from the model's prediction, and the scaling factor moves away from the predicted value. Device 01 and 02 have the same geometry and have been exposed to the same amount of FIB. However, from the quantitative analysis, device 02 seems to have experienced a larger amount of damage, reflected in by a larger drop in J_c (0) and a larger deviation in the scaling factor. Even with the same decrease in critical temperature after the patterning (0.2 K), the $J_c(0)$ for device 01 only decreased by a small amount compared to before the patterning. In comparison, device 03 has been damaged more to begin with, reflected by a smaller $J_c(0)$ value, and an α smaller than $3/2$. Additionally, the patterning on top further decreases the critical current density and moves the transition further away from perfect second order transition.

The interpretation of the fitting parameter is not definite. Device 03 already has the lowest critical temperature and critical current density after the current constriction, which indicates the damage on the device is the largest even before the current constriction has been nanopatterned. This is also evident from the critical exponent α that is very different from the predicted $3/2$ even before the second round of FIB. After the FIB nanopatterning, the value of α changed to a value a bit closer to the ideal model. However, this could be interpreted as adding randomness (partial local damage) to randomness (further damage) resulting in a new random number. This result does show the value of scaling factor α is, to some degree, an indication of how much the device is damaged by the FIB.

The scaling factor α in device 01 stays almost the same after the nanopatterning whereas it deviates by more than 0.1 for device 02, despite the change in critical temperature before and after are both 0.2 K. This indirectly suggests the damage to the superconducting properties on device 01 is more limited than it is to device 02. The question remains whether this is due to the benefit of the periodic potential, or a trivial coincidence.

7.4. DISCUSSION AND OUTLOOK

As presented in the previous section, the periodic pattern structured on the device surface with FIB does not improve the critical temperature as determined by transport measurements. The patterning also decreases the critical current. Nonetheless, when fitting the data with a scaling law, it is possible to interpret the fitting parameter as such that the damage to the device is to some degree readjusted by the benefit brought by the periodic potential. In particular when comparing the device with a periodic pattern and the devices exposed with the same dose of FIB but without periodicity, where one would expect to have the same degree of deterioration but instead one shows more damage effect from FIB than the other.

The easiest way to determine if the periodic pattern brings benefit to the devices is to increase the sample size for a statistical analysis. Unfortunately, we only have 1 device with a periodic pattern and another without. The limited sample size makes it challenging to have complete conclusions from our measurement and analysis.

Another possibility is that the periodicity of 100 nm is too large so that the periodic potential does not have the desired effect of increasing the critical temperature The patterns here were structured with 30 keV Gallium ions. According to SRIM calculations, upon vertical incidence on MgB_2, the furthest lateral distance the ion can reach is limited to about 2.5 nm, indicating the damage done on the sample is locally limited to where the beam has been. Here, we over-protected the sample by increasing distances between each milling. Based on the dose test and looking at the transport results, the distance between the line could be decreased to 80 nm. We also estimate the FIB of the 30 keV Gallium ions can resolve to at least 50 nm periodicity. However, to reach such a resolution, the risk of accidental complete removal of the top protective layer and thus completely damaging the MgB_2 sample increases strongly.

So far we have focused on the prospect of studying the effect of a periodic potential on superconductivity using transport measurements. There is a fundamental complication brought about by such a technique, despite the advantage of being relatively fast and easy; the properties measured in the experiment here are always over the whole device. If there is one weak link in the device, the measured data will only reflect the behaviour of the weak link instead of the periodically patterned part. In other words, if the critical temperature of most of the constriction goes up it only takes one small damaged area connected in series to mask this effect. One can argue that careful measurement and analysis of the data should be able to distinguish such an effect. However, this would only provide indirect evidence, especially in a situation where there are no solid estimations of how much the critical temperature and carrier density would increase. We recommend that future experiments aim at a direct local probe of the patterned area in combination with transport measurements.

Although the superconducting properties of MgB_2 potentially it an excellent candidate for this project, the epitaxially grown film might not be the best option to accommodate an imposing artificial periodic potential. Van der Waals superconductors such as $NbSe_2$ and NbS_2, which have a consistent lattice structure throughout the device might be a better candidate in this regard. We propose to have an exfoliated $NbSe_2$ flake, with contact from the bottom of the flake, and a thin layer of hBN as a protective layer on top. The hBN layer should be below 2 nm thick to ensure there can still be tunnelling of electrons during local probe measurement. The $NbSe_2$ flake should be in the order of 20-50nm thick. The periodic structure can again be patterned on the flake similarly to what was performed in this and previously reported experiments [184], namely by using FIB is used to implement damage into the superconductors instead of physically removing materials from the superconductors. However, after the transport experiment, the sample can be characterised with local probe techniques such as Conductive AFM, Kelvin Probe Force Microscopy, and if surface conditions allow, even four-probe STM. This should assist in understanding the local condition of the sample as well as provide a tool for diagnosing transport measurements.

Last but not least, we propose to use a molecular network to provide the periodic potential in a van der Waals system. As the lattice structure for a typical molecular network self-assembled on a metal surface is in the range of nm to the tens of nm, it can reach a resolution well below what can be realised by FIB. As such, it provides opportunities for improving the periodic potential length scale. However, the challenge lies in finding a compatible substrate for such networks without destroying their ability to self-assemble. This possibility will be discussed in the next chapter.

7.5. CONCLUSION

In conclusion, we studied how a periodic pattern structured by FIB influences the superconducting properties of MgB_2 devices. The measured data shows no increase in critical temperature or critical current. However, when fitting the data to the second-order-phase-transition scaling law, the fitting parameter shows a periodic pattern could potentially compensate for the damage done to the sample quality. We discussed in detail the implications of this, and gave an extensive outlook on how further research can be done on the subject.

7.A. AFM MEASUREMENTS

AFM measurement topography and profiles for the surface of device 01 and 02.

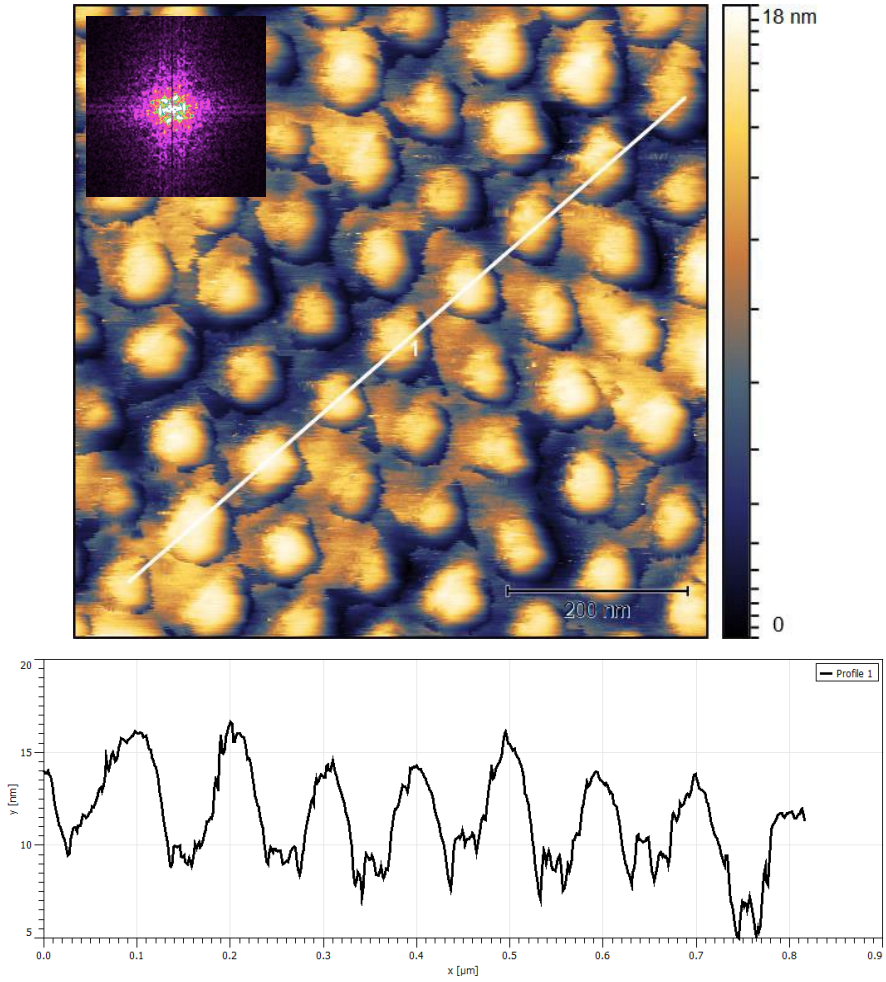

Figure 7.6: AFM measurement on top of device 1 after the periodic pattern was structured with FIB.

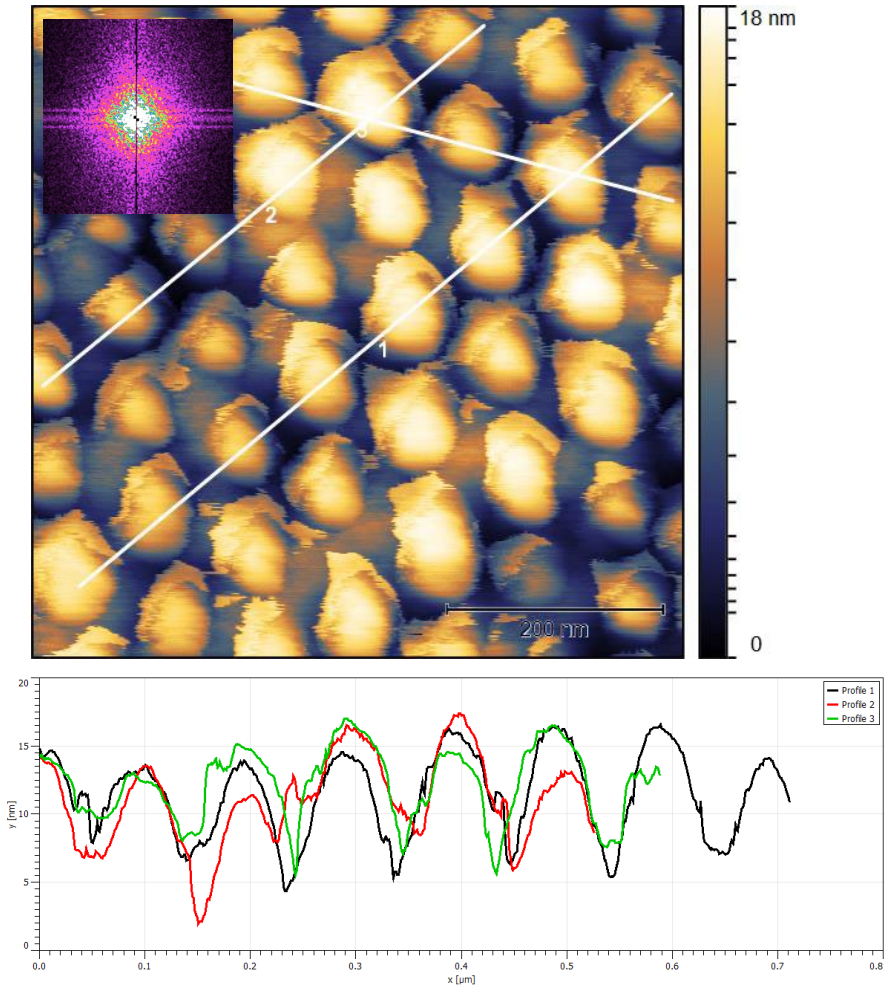

Figure 7.7: AFM measurement on top of device 2 after the non-periodic pattern was structured with FIB.

7.B. CRITICAL CURRENT DENSITY CALCULATIONS

The London penetration depth (λ) of thin film MgB_2 at zero Kevin is reported to be around 90 nm (see table 7.1). This implies that the supercurrent only flows through the edge of the microstrip in a region with a width that is proportional to the λ(T). Therefore, we estimate the critical current density of the microstrip with an effective cross-sectional area of $2\lambda(T)d$, where d = 50 nm is the thickness of the film. From the empirical scaling law $\lambda(T) = \lambda(0)/[1-(T/T_c)^2]$, at 35.5 K, λ is estimated to be between 300 and 500 nm [185]. Hence, for the constriction, the critical current densities were calculated with the actual cross-sections.